An Efficient Readout Scheme for Simultaneous Measurement From Multiple Wireless Passive *LC* Sensors

Anish Babu and Boby George, *Member, IEEE*

***Abstract*— A new readout scheme for multiple passive *LC* sensors based on the impulse response is presented here. A precharged capacitor is discharged through a readout coil which is magnetically coupled to multiple sensor coils. Fast Fourier transform of the resultant oscillatory current through the readout coil is taken, from which the equivalent impedance of the system at different frequencies is computed. The maximum value of the imaginary parts of this impedance occurs at the resonant frequencies of the sensor coils that are coupled. The conventional measurement schemes rely on a frequency sweep approach to determine the resonance frequencies of the sensor coils; that process is inherently time-consuming. A simple, low-cost readout scheme with a fast update rate is proposed. A method to measure the quality factor *Q* of the sensor coil system is also presented here. Output of the proposed scheme is independent of the variation in the coupling factor *k*. The measurement resolution of the proposed scheme has been improved using a Gaussian curve fitting approach, which also reduces the effect of noise in the final output. A prototype of the proposed system has been built with a readout coil and three sensors coupled to it and tested. The worst case error observed in the test was less than 0.5%, when the prototype system was tested with a variable capacitor (47 to 345 pF) in the sensor coil. The proposed readout scheme is useful in applications requiring simultaneous wireless monitoring of multiple physical parameters.**

***Index Terms*— Fast Fourier transform (FFT), multiple measurements, mutual inductance, passive *LC* sensor, *Q* factor.**

I. Introduction

WIRELESS passive *LC* sensors are used for non-contact measurement in several applications such as pH monitoring [1], monitoring of concrete structures [2], measurement of humidity [3], biopotential measurement [4], temperature [5], and strain [6]. They can also be used for measuring multiple physical quantities simultaneously [7], [8]. Simultaneous measurement of multiple quantities such as temperature and pH allows for temperature compensation in the measured value of pH, which in turn helps to achieve higher accuracy in the measurement [9]. A passive *LC* sensor system typically consists of a sensor coil connected to a capacitive sensor. This forms an *LC* tank circuit, whose resonance frequency (f_p) changes with change in the value of the sensor capacitance. Such sensor systems are particularly useful in applications where the physical access to the sensing element is limited. To measure the sensor parameter, a readout circuit is required. The readout circuit consists of a readout coil, which is magnetically coupled to the sensor coil. The measurement circuit, which is connected to the readout coil, measures the resonance frequency f_p of the sensor unit from which the sensor parameters (e.g., change in capacitance) can be calculated.

Phase-dip method is one of the methods used to measure the change in sensor capacitance in a wireless passive *LC* system. In [10], the phase dip of the input impedance at the resonance frequency is used to measure the sensor capacitance. To detect the phase dip, the phase at different frequencies needs to be measured. The frequency at which the phase is minimum is found to deviate from the resonance frequency, when the coupling coefficient k is large. The method proposed in [11] uses the real part of the input impedance to detect the resonance frequency. The real part of the input impedance is found to be maximum at the resonance frequency, independent of the value of k. In [12], the sensor is energized at a set of frequencies within a predetermined frequency range and the sensor responds with its own magnetic field. From the frequency, amplitude, and bandwidth of the magnetic field response the sensor parameters are determined. The methods in [10]–[12] require a frequency sweep to detect the resonance frequency. The measurement time associated with the frequency sweep does not allow to achieve fast update rates. Further, for a measurement scheme using frequency sweep, a feedback loop is required to automatically track the sensor capacitance, which is quiet complex [11]. Even though the update rate of the frequency sweep based method is low, it offers high signal-to-noise ratio (SNR) and hence a large dynamic range. A time-domain method that operates on a single frequency offers a faster update rate [13].

In [13], the phase ϕ of the input current at a frequency in the region around the sensor resonance frequency is measured. It was shown that the tangent of the phase, $\tan(\phi)$, varies linearly with the change in sensor capacitance. A real-time capacitance estimation methodology for batteryless wireless sensor systems through cascaded filtering is presented in [14]. In [15], the circuit is excited at resonance frequency and the magnitude of the reader coil current is used to compute the sensor capacitance. The magnitude of the current changes when C_2 changes, but this current is also a function of the coupling

Manuscript received July 2, 2017; revised September 1, 2017; accepted September 6, 2017. Date of publication November 22, 2017; date of current version April 5, 2018. The Associate Editor coordinating the review process was Dr. Salvatore Baglio. *(Corresponding author: Anish Babu.)*

The authors are with the Department of Electrical Engineering, IIT Madras, Chennai 600036, India (e-mail: ee14d014@ee.iitm.ac.in; boby@ee.iitm.ac.in).

Color versions of one or more of the figures in this paper are available online at http://ieeexplore.ieee.org.

Digital Object Identifier 10.1109/TIM.2017.2770858

coefficient k. It would be useful if a measurement system with the following features can be developed for wireless passive LC sensors. The features are: 1) low cost; 2) measurement time as low as possible; 3) sensitivity of the output to the variation in k is negligible; 4) hardware requirement is low; 5) ability to read from multiple sensors at the same time; 6) power required to measure is low; and 7) quality factor Q can be measured in addition to the sensor capacitance.

A new method based on fast Fourier transform (FFT) of the input current for an impulse input is proposed in [16]. A capacitor is initially charged to a predefined voltage. To measure the sensor capacitance, this capacitor is discharged through the readout coil. This is equivalent to giving an impulse input to the system. The capacitor discharges quickly, resulting in an oscillating and exponentially decaying current flow through the coil. The frequency of oscillation of the current depends on the natural frequencies of the system, one of which is the sensor parallel resonance frequency. A resistor connected in series with the readout coil gives a voltage proportional to the input current. The FFT of the voltage is taken from which the input impedance of the system is computed. For the proposed system, it has been found that the imaginary part of the input impedance is maximum at the sensor resonance frequency. The imaginary part of the input impedance for all the required frequencies is directly obtained from the proposed method. Thus, no frequency sweep is required, allowing fast update rates. The proposed method can be used to read multiple LC sensor systems simultaneously. The quality factor Q of the sensor can also be measured using the proposed approach. The output of the measurement scheme is independent of the coupling coefficient k. The mathematical model of the proposed measurement scheme and the simulation and experimental results of the proposed system are presented as follows.

II. Mathematical Model

The proposed wireless readout system can be represented by the equivalent circuit shown in Fig. 1. A capacitor C_1 is connected to a single-pole-double-throw switch S_1 as shown in Fig. 1. One terminal of the switch is connected to a dc voltage V_{in}. The other terminal is connected to the readout coil. The self-inductance and resistance of the readout coil are indicated as L_1 and R_1, respectively. The readout coil is magnetically coupled to the sensor coils. The system shown in Fig. 1 has three sensor coils. The first sensor coil has a self-inductance L_2 and resistance R_2. The capacitive sensor C_2 is connected in parallel to the sensor coil. The mutual inductance M_{12} between the sensor and the readout coils is given by $M_{12} = k_{12}\sqrt{L_1 L_2}$, where k_{12} is the coupling coefficient. Similarly, L_3 and L_4 indicate the self-inductance of the sensor coils 3 and 4. The corresponding coil resistances are R_3 and R_4, and the capacitive sensors are C_3 and C_4 in order. The resistor R_s, which is connected in series with the readout coil, acts as a current sensing resistor. To explain the operation, initially, the coil-2 alone is considered. The other sensor coils are discussed at a later stage.

Initially, switch S_1 is kept in position-0 and the capacitor C_1 is charged to a dc voltage V_{in}. To measure C_2 the switch S_1 is changed to position-1. This brings C_1 in series with L_1, R_s, and Z_{r2}. Here Z_{r2} is the secondary side impedance of sensor coil-2 expressed as a reflected impedance in the primary side and is given by (1). The capacitor C_1 discharges through L_1, R_s, and Z_{r2}. This results in an oscillatory current flow, which decays exponentially. The oscillation frequencies correspond to the natural frequencies of the system. The system, when $S_1 = 1$, has two series resonance frequencies and one parallel resonance frequency [13]. The parallel resonance frequency f_{p2} is given by $f_{p2} = 1/[2\pi\sqrt{L_2 C_2}]$

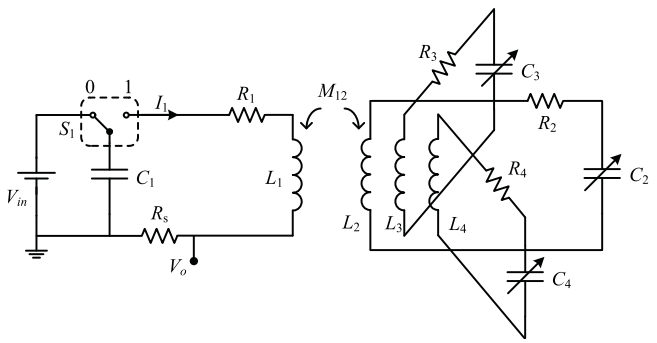

Fig. 1. Equivalent circuit of the proposed readout scheme. The mutual inductances M_{13} between L_1 and L_3 and M_{14} between L_1 and L_4 are not shown to avoid complexity in the diagram.

$$Z_{r2}(s) = \frac{-M_{12}^2 C_2 s^3}{L_2 C_2 s^2 + R_2 C_2 s + 1}. \tag{1}$$

When S_1 is at position-1, using Kirchhoff voltage law, we can write the following equation, which is written in the Laplace domain for ease of analysis

$$\frac{I_1(s)}{C_1 s} - \frac{V_{\text{in}}}{s} + L_1 s I_1(s) + R_{1eq} I_1(s) + Z_{r2}(s) I_1(s) = 0. \tag{2}$$

In (2), R_{1eq} is the sum of R_1, R_s, and the ON resistance of switch S_1. Equation (2) can be simplified to (3), where $Z(s)$ is given by (4). The impulse input results in a current flow I_1. The characteristics of the system, $Z(s)$, can be determined from the quantity $V_{\text{in}}/I_1(s)$

$$V_{\text{in}} = Z(s) I_1(s) \tag{3}$$

$$Z(s) = \frac{\prod_{n=1}^{2}\left[L_n C_n s^2 + R_n C_n s + 1\right] - M_{12}^2 C_1 C_2 s^4}{C_1(L_2 C_2 s^2 + R_2 C_2 s + 1)}. \tag{4}$$

The imaginary part of $Z(s)$, in the frequency domain, can be written as

$$Im(Z(j\omega)) = R_1\omega + \frac{\omega^5 M_{12}^2 C_2^2 R_2}{(1 - L_2 C_2 \omega^2)^2 + (\omega R_2 C_2)^2}. \tag{5}$$

The plot of the imaginary part of $Z(j\omega)$ versus frequency is given in Fig. 2. The values of the parameters used for this computation are given in Table I. The value of C_2 used was 300 pF. From Fig. 2, we can see that the imaginary part of $Z(j\omega)$ has a local maxima at the frequency where $1 - L_2 C_2 \omega^2 = 0$, which is the parallel resonance frequency

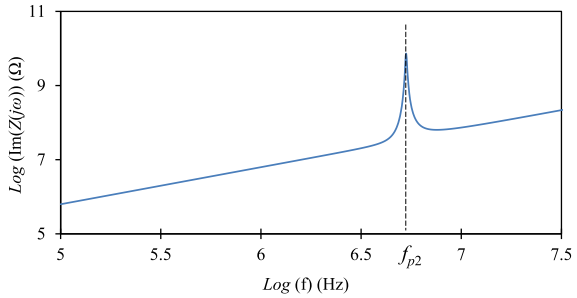

Fig. 2. Imaginary part of the impedance $Z(j\omega)$ as a function of frequency. The local maxima occur at the sensor parallel resonance frequency f_{p2}.

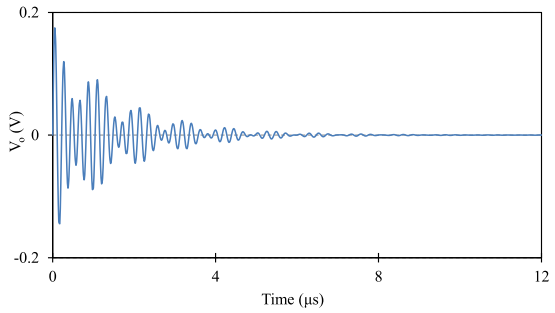

Fig. 3. Output voltage V_o obtained across the resistor R_s. This is obtained from the simulation study.

TABLE I
CIRCUIT PARAMETER VALUES

L_1	R_1	C_1	L_2	R_2	V_{in}
13.3 μH	2.9 Ω	47 pF	3.068 μH	0.7 Ω	5 V

of sensor coil-2. Thus, by measuring $Im(Z(j\omega))$, we can compute the resonance frequency and calculate C_2.

An FFT-based measurement scheme is used to determine $Im(Z(j\omega))$. In Fig. 1, the voltage V_o is given by $V_o = R_s I_1$. V_o can be decomposed to its different frequency components by taking its FFT. The voltage V_o is sampled from the instance S_1 is changed to position-1. An n-point FFT of V_o is computed where n, the number of samples of V_o taken, is a power of 2. The computed FFT consists of $n/2$ complex terms and each term V_K can be expressed in the form $V_K = \alpha_K + j\beta_K$. Here α_K is the real part and β_K is the imaginary part of the Kth term of the computed FFT output. The voltage V_o can be expressed in terms of $Z(s)$ as

$$V_o(s) = R_s I_1(s) = \frac{R_s V_{\text{in}}}{Z(s)}. \tag{6}$$

Assuming that $R_s V_{\text{in}} = 1$, the FFT components of the impedance $Z(s)$ can be computed as

$$Z_K = \frac{\alpha_K - j\beta_K}{\alpha_K^2 + \beta_K^2}. \tag{7}$$

The imaginary part of Z_K, denoted as Z_{iK}, at different frequencies is given by $-\beta_K/(\alpha_K^2 + \beta_K^2)$. Once the FFT is computed, the frequency corresponding the maximum value of Z_{iK} is identified and this is taken as f_{p2}. From f_{p2} and the known value of L_2, the value of C_2 can be computed.

Sensor coil-2 alone is considered in the above explanation. In order to use the same readout coil for multiple sensors as illustrated in Fig. 1, the resonance frequencies f_{r3} and f_{r4} of coil-3 and coil-4, respectively, should be selected in such a way that they are sufficiently apart—such that there is no cross coupling. In such a condition the Z_K and Z_{iK} for those coils can be computed as done above for sensor coil-2. The details are presented in the following section.

III. NUMERICAL STUDY AND ANALYSIS

A numerical study was conducted to: 1) verify the mathematical model and to study the effect of k and its variation; 2) determine the resolution of the measurement scheme and to develop ways to improve and test; 3) assess the effect of noise in V_o, on the FFT output; 4) verify the functionality and optimize the performance when reading multiple sensors simultaneously; and 5) test the effectiveness of the proposed Q measurement method.

A. Transient Simulation Study

A transient response of the system given in Fig. 1 was obtained, for the sensor coil-2 with L_2 and C_2, after implementing it in a MATLAB Simulink environment. The values of the parameters used for the study are given in Table I. These values are taken from the prototype developed to experimentally evaluate the proposed scheme. The coupling coefficient k was kept at 0.1. The value of C_2 used was 330 pF. The capacitor C_1 was given an initial voltage of 5 V. At time $t = 0$, the capacitor was discharged through the readout coil L_1. The resulting current flow in the circuit was measured by sensing the voltage V_o across the resistor R_s. The voltage V_o observed is given in Fig. 3. The sampling frequency was set at 40 MHz.

An 8192 point FFT of V_o was computed. As can be seen in Fig. 3, the amplitude of voltage V_o decays exponentially with time. The FFT windowing function should not attenuate the initial portion of the signal. Therefore, a rectangular window was chosen for the FFT computation. From the FFT output, the Z_K was calculated using (7). The resulting imaginary part, Z_{iK}, at different frequencies obtained is given in Fig. 4. The maximum value of Z_{iK} is observed at the frequency very close to f_{p2}. This was repeated for different values of k. The peak value of Z_{iK} always occurred at the same frequency indicating that the proposed scheme is independent of the value of the coupling factor k. The highest frequency component in the FFT output is equal to half the sampling frequency F_s at which the signal is acquired. The resonance frequency of the sensor coil should remain lower than $F_s/2$. Therefore, the sampling rate of the analog to digital converter (ADC) determines the range of the resonance frequency that can be determined by the proposed scheme. In the simulation study, the signal V_o was sampled at four times the maximum sensor resonance frequency.

B. Resolution of the Measurement Scheme

The FFT output Z_{iK} gives the magnitude of the imaginary part for discrete frequency values (bins). From this, the

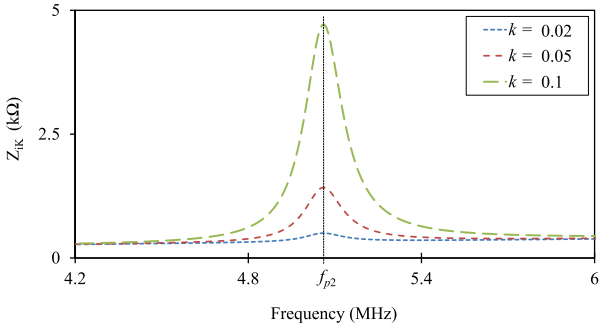

Fig. 4. Imaginary part, Z_{iK}, of the FFT for different values of coupling factor k. The peak value of Z_{iK} occurs at the same frequency independent of the value of k.

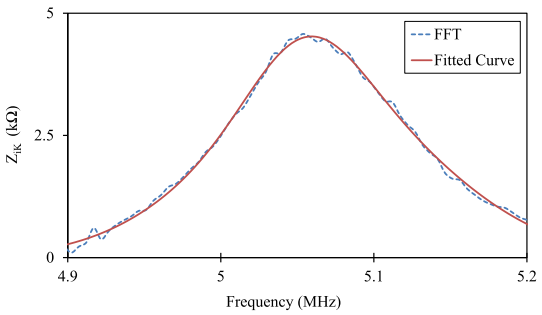

Fig. 5. Imaginary part of the FFT, Z_{iK}, when noise was added to the input signal. The fit two-term Gaussian curve is also shown. The value of f_{p2} detected with and without curve fit were 5.057 and 5.051 MHz, respectively. The true value of f_{p2} was 5.059 MHz.

TABLE II
PARAMETER VALUES [3]

L_2 (μH)	C_2 range (pF)	f_{p2} range (MHz)
6	180 – 240	4.843 – 4.194

frequency corresponding to the maximum value is taken as f_{p2}. Therefore, the sensor capacitance values computed using this method will also be discrete in nature. Thus, the resolution of the measurement system depends on the size of the frequency bin. Let the sampling frequency be F_s and the number of samples taken for computing the FFT be N_s. Then, the FFT output will have $N_s/2$ frequency bins and the size of each frequency bin is given by $f_{\text{bin}} = F_s/N_s$. For a small change ΔC_2 in C_2, the change in resonance frequency Δf_{p2} is given by $\Delta f_{p2} = f_{p2}\Delta C_2/2C_2$ [13]. The frequency bin size f_{bin} is the minimum change in f_{p2} that can be detected by the measurement scheme. Therefore, the measurement resolution of C_2 is given by $2f_{\text{bin}}C_2/f_{p2}$.

Consider a typical wireless passive LC sensor system, whose parameter values are shown in Table II. Let the sampling frequency be 40 MHz and the number of samples taken for FFT is 8192. Therefore, the size of each frequency bin, f_{bin}, will be 4.88 kHz. For these specifications and sensor parameters, the resolution of the measurement scheme will be 0.56 pF (if the other errors are neglected). The total change in f_{p2} for the full-scale change in C_2 is 649 kHz. Therefore, there will be 649/4.88 = 133 discrete output values over the full range of sensor C_2. A method to improve the resolution, without additional hardware is presented below.

C. Improved Measurement Resolution

As discussed above, the resolution of the proposed measurement scheme is limited by the size of the frequency bin of the FFT. As the shape of the Z_{iK} versus frequency curve is known (see Fig. 4), the resolution can be improved significantly by fitting the Z_{iK} data to a two-term Gaussian curve as illustrated in Fig. 5. The Z_{iK} data shown in Fig. 5 has intentionally included noise (the details are discussed below). The fit curve had an R^2 value of 0.998. From this fit curve, the frequency corresponding to the maximum value of Z_{iK} can be determined at a much higher resolution as the curve is continuous. This significantly improves the resolution of the measurement scheme. The measurement resolution is now limited only by the noise in the signal V_o.

TABLE III
EFFECT OF NOISE

	N_s	ADC SNR (dB)	Measured C_2 (pF)	Standard Deviation (pF)
Without Gaussian fit	8192	No noise	179.74	0
	8192	80	179.8	0.65
With Gaussian fit	8192	80	180.05	0.18
	2048	80	180.12	0.20
Note: The value of C_2 is set as 180 pF. The sampling frequency was 40 MHz.				

D. Effect of Noise

The real-world signal V_o will have noise due to different sources. Digitization of the signal will also introduce quantization noise in the digitized V_o. To study the effect of noise on the final output, an appropriate amount of noise was added to the voltage V_o obtained from the simulation, and the performance was studied. The ADC used in the prototype developed had an effective number of bits (ENOB) of 13.5 b. In the simulation study, the signal V_o was first quantized using a 13-b quantizer. Then, Gaussian white noise was added to the signal V_o, to make the SNR of the signal as 76 dB, such that the standard deviation in the computed value of C_2 from the simulation study matched with the experimental results. The two-term curve fitting approach was not used in both these studies. The FFT components Z_{iK} after the noise was added to the signal is given in Fig. 5. From Fig. 5, it can be seen that there are multiple minor peaks around the region near f_{p2} compared to the smooth curve obtained from a noise-free signal earlier. Therefore, the frequency bin corresponding to the maximum value of Z_{iK} can be different from actual f_{p2}. To detect the peak accurately, a two-term Gaussian curve was fit to the plot of Z_{iK}. As can be seen in Fig. 5, the same approach used to improve the resolution of the measurement helps to remove the multiple peaks in Z_{iK} in the region around f_{p2}.

The above-mentioned approach was simulated under different conditions as given in Table III. The value of C_2 was set as 180 pF, and under each condition C_2 was computed 12 times.

When the signal V_o had no noise, the standard deviation in the measurement of C_2 was zero. But when noise was added to the signal, a standard deviation of 0.65 pF was observed in the computed value of C_2. The seed for the Gaussian noise generator was varied each time so that the noise signal is not repeated in the study. The standard deviation in the computed C_2 reduced significantly when the Gaussian fitting was used. Further, the performance of the proposed measurement scheme was not affected when the FFT size was reduced by a factor of 4. Thus, fitting a two-term Gaussian curve to the plot of Z_{iK} gave the following advantages: 1) the standard deviation of the measurement improved which in turn improved the measurement resolution and 2) the FFT size can be reduced without affecting the performance of the measurement scheme.

E. Reading Multiple Sensors

The numerical study has been extended to the case of reading from multiple numbers of passive LC sensors as illustrated in Fig. 1. Each of the sensor coils has a frequency range over which its resonance frequency varies as the value of the sensing parameter changes. There should be a sufficient gap between the frequency ranges (resonant frequency and its change) of the sensor coils to avoid any cross coupling. Simulation studies showed that, to fit a two-term Gaussian curve to the plot of Z_{iK}, the values of Z_{iK} over a frequency range $f_p \pm 0.15$ MHz is required, for the prototype designed. The resonance frequency of sensor coil-3 is f_{p3} and let $f_{p3} > f_{p2}$ as in Fig. 6. For the readout circuit, to be able to measure the entire range of both the sensor coils, there should be a gap of 0.3 MHz between the maximum value of f_{p2} and the minimum value of f_{p3}.

Three sensor coils were considered for the simulation study. In addition to the parameters given in Table I, $C_2 = 270$ pF, $C_3 = 200$ pF, $C_4 = 150$ pF, $L_3 = L_4 = 3$ μH, and $k_{12} = k_{13} = k_{14} = 0.1$ were used for the study. To measure the sensor capacitor values, S_1 is changed to position-1. Quantization noise and Gaussian white noise was added to the voltage V_o. The SNR value of V_o is now 76 dB. From the FFT of V_o, the FFT components Z_{iK} was computed. The plot of Z_{iK} when three sensor-coil combinations are placed near the readout coil is shown in Fig. 6. As can be seen from the figure, there are three peaks corresponding to the three resonance frequencies that are easily distinguishable, correctly. When multiple sensor coils are used, the coupling between the sensor coils slightly shifts the resonance frequency of the LC sensor. The sensor coils should be placed such that the coupling between them is very small. In the simulation study, for the value of the parameters used (equivalent to the prototype), a coupling coefficient of less than 0.02 between the sensor coils was found to have negligible effect on the output.

The L_1 and C_1 in the readout circuit acts as an equivalent bandpass filter with center frequency f_r given by $f_r = 1/\sqrt{L_1 C_1}$. Due of this, in V_o, the magnitude of the frequency components near f_r is high, while that for the frequency components away from f_r is low. Therefore, the effect of noise will be more in the frequency range away from f_r. The same can be noticed in the plot of Z_{iK} given in Fig. 6. Here $f_r = 6.4$ MHz. The plot of Z_{iK} in the region near f_r is a smooth curve and the measurement scheme gave good results when the sensor coil frequency was near f_r. This limits the effective frequency range over which the resonance frequency of the sensor coils can vary, which in turn determines the number of sensor coils that can be measured simultaneously.

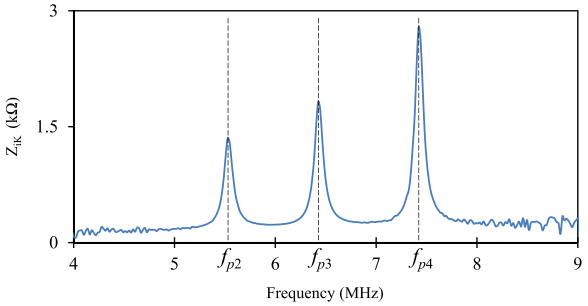

Fig. 6. Imaginary part Z_{iK} of the FFT when the readout coil is coupled to three LC sensors as illustrated in Fig. 1.

F. Measurement of Quality Factor Q

In a number of wireless LC sensing applications, the measurement of the quality factor Q of the sensor coil part is required [9]. The proposed method can be used to measure the Q factor of the sensor system. The Q factor of a passive LC sensor system with coil-2 (i.e., L_2, C_2, and R_2) is given by $Q = (1/R_2)(L_2/C_2)^{(1/2)}$. Thus, once Q is measured, the value of the resistive element in the sensor can be computed. A resistive sensor, say, a thermistor can be connected in parallel with C_2. This resistor comes in parallel with the leakage resistance of the sensor capacitor C_2. The effective parallel resistance, R_{p2}, can be expressed as an equivalent series resistance $R_{p2}/(1+(\omega R_{p2} C_2)^2)$. This is in series with the sensor coil resistance R_2, and can be estimated from the measured value of Q factor.

$$Z_{\rm so}(j\omega) = \frac{1}{(1-L_2C_2\omega^2)+j\omega R_2 C_2} \tag{8}$$

$$|Z_{\rm so}(j\omega)| = \frac{1}{\sqrt{(1-L_2C_2\omega^2)^2+(\omega R_2C_2)^2}} \tag{9}$$

$$Im(Z_{\rm so}(j\omega)) = \frac{\omega R_2 C_2}{(1-L_2C_2\omega^2)^2+(\omega R_2C_2)^2}. \tag{10}$$

Consider a second order impedance $Z_{\rm so}$ given by (8). The magnitude of $Z_{\rm so}$ can be written as in (9). Fig. 7 shows the plot of $|Z_{\rm so}(j\omega)|$. Here f_1 and f_2 are the frequencies corresponding to the half-power points (-3 dB points). The bandwidth of the system is given by $f_{\rm bw} = f_2 - f_1$. The Q factor of the system can be calculated as $Q = f_{p2}/f_{\rm bw}$. The imaginary part of $Z_{\rm so}$ can be expressed as in (10). The denominator term of $Im(Z_{\rm so}(j\omega))$ is the square of the denominator term of $Z_{\rm so}$ given in (9). Therefore, the bode plot of $Im(Z_{\rm so}(j\omega))$, in the logarithmic scale, will be the plot of $Z_{\rm so}(j\omega)$ scaled by a factor of two and then multiplied by the numerator term. The two frequencies f_1 and f_2 will now appear at the -6 dB points in the graph of $Im(Z_{\rm so}(j\omega))$.

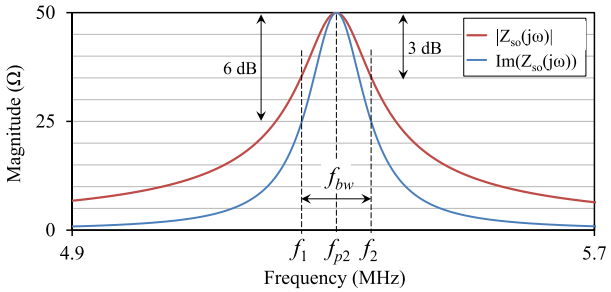

Fig. 7. Magnitude plot of $Z_{so}(j\omega)$ and the plot of $Im(Z_{so}(j\omega))$. The value of f_{bw} computed from both the plots are the same.

Here, it is assumed that the change in the numerator term of (10) over the frequency range f_{bw} is small. The frequency corresponding to the peak value remains the same. Therefore, the Q factor can be measured from the graph of $Im(Z_{so}(j\omega))$, using the values of f_1 and f_2 measured at the -6 dB points. $Im(Z_{so}(j\omega))$ can be estimated from the plot of Z_{iK}. To verify this, a simulation study was conducted. The Q factor of the LC sensor was varied and from the plot of Z_{iK}, the Q was measured. The measured value of Q matched with the true value of Q.

IV. Experimental Setup and Results

A. Prototype Unit

A prototype of the proposed scheme was developed and tested experimentally to validate its performance. A planar coil of dimension 20 mm × 20 mm with 10 turns was used as the sensor coil. A coil of dimension 70 mm × 60 mm with 10 turns was selected as the readout coil. Both the coils were fabricated on a printed circuit board. The inductance and resistance values of these coils are given in Table I. The switch S_1 in the circuit given in Fig. 1 was realized using MAX4624 IC. The switch parameters had a significant effect on the transient characteristics of the system. The switch had a charge injection of 65 pC, which was comparable to the initial charge stored in C_1. Therefore, the circuit was modified (functionally equivalent to the circuit in Fig. 1) as shown in Fig. 8. The capacitance C was realized by a capacitor of value 100 μF. This comes in series with C_1 and the effective capacitance is close to C_1 (assuming that the resistance R is very large compared to the opposition to current flow introduced by L_1, C_1, R_1, Z_r, and R_s. A resistor $R = 330\ k\Omega$ was connected from the terminal 1 of S_1 to ground. This provides a path for the C_1 to discharge when S_1 is changed to position-0. To digitize the voltage V_o, a 16-b ADC, ADS5560 from Texas Instruments Incorporated, Dallas, TX, USA, was used. A data capture card TSW1405EVM was used to read the data from the ADC through a low-voltage differential signaling interface and transfer it to a personal computer. A photograph of the experimental setup is given in Fig. 9.

B. Functionality Test

In this test, the accuracy of the measurement scheme while reading the change in capacitance of a sensor capacitor C_2 was

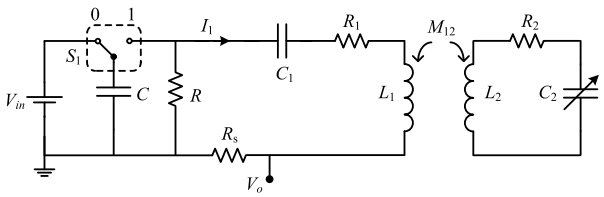

Fig. 8. Equivalent circuit of the modified readout scheme.

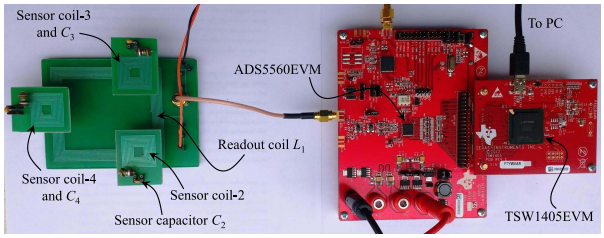

Fig. 9. Photograph of the experimental setup.

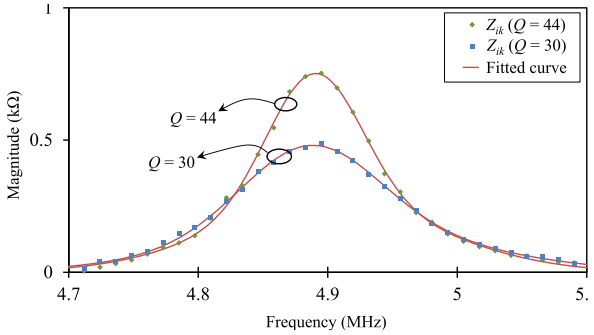

Fig. 10. FFT components Z_{iK} obtained from the experimental setup. The fit two-term Gaussian curve is also shown. The plot of Z_{iK} for a lower value of Q factor is also given.

tested. The sensor coil was kept on the top of the readout coil and the coupling coefficient k was measured as 0.08. Initially the capacitor C was charged to 5 V. Initial value of C_2 was 344.7 pF. To measure C_2, S_1 was changed to position-1. The voltage V_o was sampled from the instant when S_1 was changed to position-1. The sampling frequency was set at 40 MHz and 2048 samples of V_o were recorded. A 2048 point FFT of the sampled data was computed using MATLAB. From the FFT output, the components Z_{iK} were calculated. The plot of Z_{iK} versus frequency obtained is given in Fig. 10. After fitting a two-term Gaussian curve, the frequency corresponding to the peak value of Z_{iK} was obtained. This was taken as the resonance frequency f_{p2} from which the value of C_2 was calculated. For the selected value of sampling frequency and number of samples, the size of frequency bin is 19.52 kHz. The resolution of the measurement setup for this set of L_2 and C_2 is 1.2 pF. This is the resolution without the fitting approach. After implementing the Gaussian fit, the resolution is limited only by the noise in the input signal V_o.

The value of C_2 was then varied from 47 to 345 pF. The actual values of C_2 were measured using an HP 4724 LCR meter, which has an accuracy of 0.1%. The plot of the measured value of C_2 versus the actual value of C_2 is given

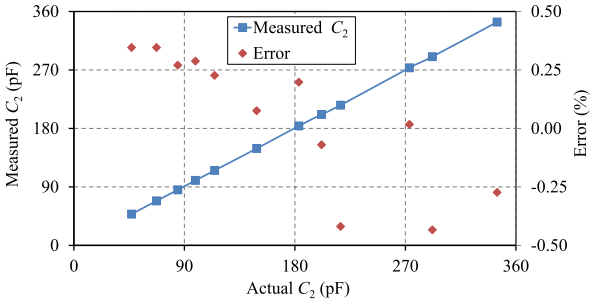

Fig. 11. Measured value of C_2 connected in the sensor coil versus the actual value of C_2.

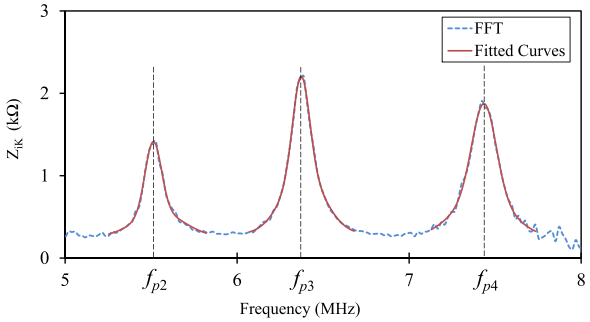

Fig. 12. Imaginary part of the FFT, Z_{iK} when reading three *LC* sensors simultaneously. The three fit two-term Gaussian curves are also shown.

TABLE IV
EFFECT OF CHANGE IN k

k	0.03	0.04	0.048	0.07	0.106	0.125
C_2 (pF)	149.2	148.6	148.9	149.3	148.9	148.8

in Fig. 11. The worst case error was found to be less than 0.5%. To test the repeatability of the measurement scheme, each value of C_2 was measured 12 times and the maximum value of standard deviation in the measurement was found to be 0.24 pF.

C. Effect of Variation in k

The effect of variation in k in the measured output was studied in this test. A 148.8-pF fixed value capacitor was used as C_2. Initially, the sensor coil was kept on the top of the readout coil as shown in Fig. 9. The coupling coefficient k was then varied by changing the position of the sensor coil with respect to the readout coil. The capacitance C_2 was measured for different values of k and is given in Table IV. As can be seen, the measured value of C_2 was not affected when k was changed from 0.03 to 0.125. Therefore, the proposed measurement scheme is independent of the value of k.

D. Measuring Multiple Sensors Simultaneously

To test the performance of the measurement scheme while measuring multiple *LC* sensors, three *LC* sensors were kept magnetically coupled to the readout coil. Each sensor coil had a self-inductance of about 3 μH. Three capacitors of values 273.3, 201.7, and 148.8 pF were used as sensor capacitors. The readout circuit is the same as the one used in Section IV-B when a single sensor capacitance was measured. As usual, S_1 was changed to position-1, and from the voltage V_o the FFT components Z_{iK} were computed. The plot of Z_{iK} versus the frequency obtained is given in Fig. 12. As can be seen in Fig. 12, there are three peaks in the plot of Z_{iK} corresponding to the three resonance frequencies. As explained earlier, to estimate the resonance frequency with a higher resolution, a two-term Gaussian curve was fit to the section of the plot around the peak value. This was done for all the three resonant peaks. The fit curves are shown in Fig. 12. From the fit curve, the individual resonance frequencies were measured as 5.498, 6.392, and 7.438 MHz, respectively. The measured values of the sensor capacitors were 272.5, 202.2, and 149.3 pF. Next, the value of C_2 was varied, keeping C_3 and C_4 constant. The measured value of C_2 was found to match with the actual value. The worst case error in the measurement of the sensor capacitance was less than 0.5%, similar to the results obtained when sensor coil-2 alone was measured.

TABLE V
QUALITY FACTOR MEASUREMENT

R_L	Actual Q	Measured Q
56 kΩ	42.69	42.48
33k kΩ	40.88	40.36
22 kΩ	38.32	37.74
15 kΩ	35.77	35.16
10 kΩ	31.81	32.43
8.2 kΩ	30.22	30.02
7.5 kΩ	29.13	28.45
5.2 kΩ	27.03	26.95

E. Measurement of Quality Factor Q

The Q factor of the sensor was measured using the method described in Section III-F. A 344.7-pF capacitor was used as C_2. The coupling factor k was measured as 0.08. A resistor R_L was connected across C_2, and the value of R_L was changed to vary Q. The plot of Z_{iK} for two different values of Q recorded is given in Fig. 10. The change in Q is clearly visible in Fig. 10. The true value of Q was estimated using a network analyzer. The measured value of Q and its true value for different values of R_L is given in Table V. The measurement of Q involved the estimation of three frequencies f_1, f_2, and f_{p2}. The errors in the estimation of each of those frequencies resulted in additional error in the measurement of Q compared to the measurement of sensor capacitance where only single frequency was measured. The Q measurement results showed that the scheme is useful, for example, in applications where temperature compensation of the measured quantity is desired [9], [17].

In the proposed scheme, to measure C_2, S_1 is changed to position-1 and 2048 samples of V_o are taken. When sampled at 40 MHz, this takes about 50 μs. A 2048 point FFT can be computed in about 150 μs [18]. The time taken for the computation of C_2 and the Q factor from the FFT output depends on the speed of the processing unit. These computations can take place as a parallel process while the measurement unit samples the voltage V_o again. Thus very fast update rates are possible using the proposed scheme. In the frequency sweep approach,

the circuit is excited at one frequency and measurements are taken. This process is repeated at different frequencies from which f_p is computed. A sudden modification in excitation frequency results in a transient response which can influence the measurement of f_p. The transient period can be as high as 150 μs [19]. In such a case, the time taken to measure C_2 = (range of the frequency sweep/frequency change step size) $\times$ 150 μs. To compute Q factor, three frequencies f_1, f_2, and f_p need to be identified for which the range of the frequency sweep has to be extended to include all the three frequencies. The time required to read from multiple sensors will be much higher. In the proposed scheme, multiple sensors can be read in a single measurement cycle.

V. Discussion and Conclusion

A simple, low-cost measurement scheme capable of measuring from multiple passive LC sensors is presented. Three LC sensors were measured simultaneously using the proposed method. The change in the capacitance of the sensor connected to the sensor coil can be measured in a single impulse measurement excitation, thereby reducing the measurement time. The readout circuit is simple as no complex feedback loops are required to track the sensor capacitance continuously compared to measurement schemes that rely on frequency sweep approach [11]. The measured output was not affected when the coupling coefficient k was varied by about $\pm$50% from its initial value of 0.08. A method to measure the Q factor of the sensor is also proposed which is useful for temperature compensated measurement of physical quantities such as pH, humidity, and pressure. A prototype of the proposed scheme has been developed and tested. The worst case error was found to be less than 0.5%. The excitation circuit sends a nearly impulse-like current through the readout coil, with an energy per measurement cycle in the range of 2.5 μJ. The hardware required in the readout is low as no sweep frequency source is required, unlike the conventional schemes. The total energy requirement can be kept low by using low power ADCs and FFT computing processors. A 2048 point FFT can be completed in about 150 μs consuming about 6 μJ [18]. The transient current which flows through the readout coil dies down within tens of microseconds and the update rate is limited only by the FFT computation time.

References

[1] S. Bhadra *et al.*, "Fluid embeddable coupled coil sensor for wireless pH monitoring in a bioreactor," *IEEE Trans. Instrum. Meas.*, vol. 63, no. 5, pp. 1337–1346, May 2014.

[2] K. Perveen, G. E. Bridges, S. Bhadra, and D. J. Thomson, "Corrosion potential sensor for remote monitoring of civil structure based on printed circuit board sensor," *IEEE Trans. Instrum. Meas.*, vol. 63, no. 10, pp. 2422–2431, Oct. 2014.

[3] T. J. Harpster, S. Hauvespre, M. R. Dokmeci, and K. Najafi, "A passive humidity monitoring system for *in situ* remote wireless testing of micropackages," *J. Microelectromech. Syst.*, vol. 11, no. 1, pp. 61–67, Feb. 2002.

[4] J. Riistama, E. Aittokallio, J. Verho, and J. Lekkala, "Totally passive wireless biopotential measurement sensor by utilizing inductively coupled resonance circuits," *Sens. Actuators A, Phys.*, vol. 157, no. 2, pp. 313–321, 2010.

[5] D. Marioli, E. Sardini, and M. Serpelloni, "Passive hybrid MEMS for high-temperature telemetric measurements," *IEEE Trans. Instrum. Meas.*, vol. 59, no. 5, pp. 1353–1361, May 2010.

[6] M. Bona, M. Serpelloni, E. Sardini, C. O. Lombardo, and B. Andò, "Telemetric technique for wireless strain measurement from an inkjet-printed resistive sensor," *IEEE Trans. Instrum. Meas.*, vol. 66, no. 4, pp. 583–591, Apr. 2017.

[7] Q. Y. Ren, L. F. Wang, J. Q. Huang, C. Zhang, and Q. A. Huang, "Simultaneous remote sensing of temperature and humidity by LC-type passive wireless sensors," *J. Microelectromech. Syst.*, vol. 24, no. 4, pp. 1117–1123, Aug. 2015.

[8] Q. Tan, T. Luo, T. Wei, J. Liu, L. Lin, and J. Xiong, "A wireless passive pressure and temperature sensor via a dual LC resonant circuit in harsh environments," *J. Microelectromech. Syst.*, vol. 26, no. 2, pp. 351–356, Apr. 2017.

[9] S. Bhadra, D. S. Y. Tan, D. J. Thomson, M. S. Freund, and G. E. Bridges, "A wireless passive sensor for temperature compensated remote pH monitoring," *IEEE Sensors J.*, vol. 13, no. 6, pp. 2428–2436, Jun. 2013.

[10] K. Bao *et al.*, "A readout circuit for wireless passive LC sensors and its application for gastrointestinal monitoring," *Meas. Sci. Technol.*, vol. 25, no. 8, p. 085104, 2014.

[11] R. Nopper, R. Has, and L. Reindl, "A wireless sensor readout system—Circuit concept, simulation, and accuracy," *IEEE Trans. Instrum. Meas.*, vol. 60, no. 8, pp. 2976–2983, Aug. 2011.

[12] S. E. Woodard and B. D. Taylor, "Measurement of multiple unrelated physical quantities using a single magnetic field response sensor," *Meas. Sci. Technol.*, vol. 18, no. 5, pp. 1603–1613, 2007.

[13] A. Babu and B. George, "A linear and high sensitive interfacing scheme for wireless passive LC sensors," *IEEE Sensors J.*, vol. 16, no. 23, pp. 8608–8616, Dec. 2016.

[14] H. S. Kim, S. Sivaramakrishnan, A. S. Sezen, and R. Rajamani, "A novel real-time capacitance estimation methodology for battery-less wireless sensor systems," *IEEE Sensors J.*, vol. 10, no. 10, pp. 1647–1657, Oct. 2010.

[15] H. Zhang, Y. Hong, B. Ge, T. Liang, and J. Xiong, "A novel readout system for wireless passive pressure sensors," *Photon. Sens.*, vol. 4, no. 1, pp. 70–76, 2014.

[16] A. Babu and B. George, "An FFT based readout scheme for passive LC sensors," in *Proc. IEEE I2MTC*, Turin, Italy, May 2017, pp. 669–673.

[17] M. Rocznik, F. Henrici, and R. Has, "ASIC for a resonant wireless pressure-sensing system for harsh environments achieving $\pm$2% error between $-$40 and 150 °C using Q-based temperature compensation," in *IEEE Int. Solid-State Circuits Conf. (ISSCC) Dig. Tech. Papers*, San Francisco, CA, USA, Feb. 2012, pp. 202–204.

[18] M. McKeown, (2013). "FFT implementation on the TMS320VC5505, TMS320C5505, and TMS320C5515 DSPs," Texas Instrum. Dallas, TX, USA. Appl. Rep. SPRABB6B. [Online]. Available: http://www.ti.com/lit/an/sprabb6b/sprabb6b.pdf

[19] R. J. F. de Oliveira and P. J. Abatti, "Analysis of telemetric system based on remote resonant sensing circuit," *Electron. Lett.*, vol. 42, no. 13, pp. 750–752, Jun. 2006.

Anish Babu was born in Kottayam, India, in 1987. He received the B.Tech. degree in electrical and electronics engineering from the National Institute of Technology, Calicut, India, in 2010, and the M.Tech. degree in electrical engineering from IIT Madras, Chennai, India, in 2014, where he is currently pursuing the Ph.D. degree in sensors and instrumentation.

His current research interests include sensors, measurements, and instrumentation.

Boby George (M'07) was born in Kannur, India, in 1977. He received the M.Tech. and Ph.D. degrees in electrical engineering from IIT Madras, Chennai, India, in 2003 and 2007, respectively.

He was a Post-Doctoral Fellow with the Institute of Electrical Measurement and Measurement Signal Processing, Technical University of Graz, Graz, Austria, from 2007 to 2010. He joined the faculty of the Department of Electrical Engineering, IIT Madras, in 2010, where he is currently an Associate Professor. His current research interests include measurements, sensors, and instrumentation.